

LETTER TO THE EDITOR

EWOCS-V: Is Wd1-72 a recent post-interaction WR+O binary?

C. J. K. Larkin^{1,2,3}, J. Mackey⁴, H. Jin⁵, A. A. C. Sander^{2,6}, B. Reville¹, K. Anastasopoulou⁷, M. Andersen⁸, A. Bayo⁸, J. J. Drake⁹, E. K. Grebel², M. G. Guarcello⁷, T. J. Haworth¹⁰, V. M. Kalari¹¹, R. R. Lefever², F. Najarro¹², B. W. Ritchie¹³, and E. Sabbi¹¹

(Affiliations can be found after the references)

Received DATE; accepted DATE

ABSTRACT

The evolutionary origin of Wolf-Rayet (WR) stars at Solar metallicity is unclear. Single-star evolution from massive O stars, possibly via a Luminous Blue Variable phase, is challenged by binary period distributions of different WR subtypes. Wd1-72 is a WN7b+O binary embedded in the collective wind of the Galactic young massive cluster Westerlund 1 (Wd 1). It is surrounded by highly structured nebulosity, with cometary tails pointing away from Wd 1 and quasi-spherical droplets towards it. In this letter, we demonstrate that this morphology can be qualitatively reproduced by a hydrodynamic simulation of non-conservative Roche Lobe Overflow (RLOF) mass-loss into a cluster wind. Our model is based on a detailed binary evolution track consistent with key known properties of Wd1-72. Our work suggests Wd1-72 could be only ~ 10 kyr post-RLOF, and the hydrogen-free nature of Wd1-72 favours this being a second or subsequent RLOF episode. Follow-up observations could make Wd1-72 a valuable benchmark for probing mass-loss and mass-transfer in forming gravitational-wave binary-progenitor systems.

Key words. Hydrodynamics – Stars: winds, outflows – Stars: Wolf-Rayet – Stars: binaries: close – Stars: circumstellar matter

1. Introduction

In the classical single-star scenario proposed by [Conti \(1975\)](#), massive O stars undergo intense mass-loss (\dot{M}), stripping the hydrogen (H) envelope and producing a Wolf-Rayet (WR) star. This may apply to the most massive stars ($M_{\text{init}} \gtrsim 100 M_{\odot}$, e.g., [Sabahit et al. 2022](#)), but steady winds alone are potentially insufficient to do this for a wider range of initial masses. A brief Luminous Blue Variable (LBV) phase with eruptive \dot{M} has therefore been suggested ([Langer et al. 1994](#)) and is applied in grids of massive-star evolution models (e.g., [Ekström et al. 2012](#)). In such evolution models, the resulting WR stars usually begin with a nitrogen-rich surface (WN-type) of a late subtype and then pass gradually to earlier subtypes and eventually to the carbon-rich WC stage (e.g. [Groh et al. 2014](#)). However, while there are a few observations of transitional WN/WC and even WN/WO stars (e.g., [Conti & Massey 1989](#); [Sander et al. 2025](#)), the single-star nature of larger LBV eruptions has been questioned (e.g., [Boffin et al. 2016](#); [Hirai et al. 2021](#)).

The majority of massive stars are in multiple systems and will experience some binary interaction in their lifetime (e.g. [Sana et al. 2012](#); [de Mink et al. 2014](#)). Such effects have long been suggested as an alternative path to strip away enough of the outer envelope to form a WR star (e.g. [Paczynski 1967](#)). Binary stripping could also break the presumption of self-stripping where WR stars form as (very) late WN subtypes and then consecutively evolve to earlier ones. [Dsilva et al. \(2023\)](#) showed that the Galactic WN binary population have mostly short periods (1–10 d) whereas the WC population distribution peaks at ~ 5000 d. This implies their formation pathways are different, leaving many open questions about descendants of these systems. This has implications for not only our understanding of WR formation, but also the properties of the progenitors of gravitational waves from black-hole binary mergers (e.g. [Higgins et al. 2021](#); [Marchant & Bodensteiner 2024](#)).

The young massive cluster Westerlund 1 (Wd 1) is an ideal laboratory to study massive stellar evolution due to its large, diverse and likely coeval (age ~ 6 Myr, [Castellanos et al. in prep.](#), although this is debated by e.g. [Beasor et al. 2021](#)) population of massive stars. This includes 24 WR stars (>90% of which are binaries, [Crowther et al. 2006](#); [Anastasopoulou et al. 2024](#)) as well as the sgB[e] star Wd1-9 ([Clark et al. 2020](#)), likely a WR+OB binary system that recently experienced Case-B mass transfer ([Anastasopoulou et al. 2025](#)). JWST observations of Wd 1 by the Extended Westerlund 1 and 2 Open Clusters Survey (EWOCS) collaboration show the cluster is surrounded by complex nebulosity ([Guarcello et al. 2025](#))—a finding unexpected for a cluster this old because feedback should disperse leftover natal gas on much shorter timescales ([Portegies Zwart et al. 2010](#)).

In the west and south of Wd 1, the nebulosity appears to be embedded in a collective radially expanding cluster wind, driven by the powerful WR stars in the core. In the east however, the cometary-like droplets appear to be centered on Wd1-72, a WN7b + late O supergiant binary system (alias WR A or WR 77sc) with two periods observed. A 7.63 d period (P) was reported by [Bonanos \(2007\)](#) in optical data and also observed in X-rays by [Anastasopoulou et al. \(2024\)](#), who found an additional stronger P of 81 d. The X-ray spectrum of Wd1-72 is very similar to that of Wd1-9 ([Clark et al. 2008](#); [Anastasopoulou et al. 2024](#)). Wd1-72 is also a binary with both components similar to the Wd1-9 model proposed by [Anastasopoulou et al. \(2025\)](#), who suggest it as an analogue for the near future of Wd1-9.

In this letter, the fifth in the EWOCS series, we demonstrate how both key aspects of the qualitative morphology of the nebulosity around Wd1-72 as seen at $11\mu\text{m}$ can be reproduced with a hydrodynamic model of intense non-conservative Roche Lobe Overflow (hereafter RLOF) \dot{M} into a cluster wind. The \dot{M} properties are motivated by a bespoke binary stellar evolution track consistent with the known properties of Wd1-72. We briefly discuss implications for massive binary evolution, and how follow-

up observations are required to constrain the recent \dot{M} history, and test the possible post-interaction nature of, Wd1-72. Our letter is organised as follows: In Sect. 2 we describe our simulation setup. In Sect. 3 we present our simulation and compare it qualitatively with JWST observations. We discuss our findings and present our conclusions in Sect. 4. In the appendices we show how our evolutionary track compares to the measured properties of Wd1-72 (App. A), why a giant LBV eruption cannot explain the observations (App. B), and estimates of dust emission from the dense clumps produced in the simulation (App. C).

2. Methods

2.1. MESA evolutionary track

We use a newly computed MESA (version 10398, Paxton et al. 2011, 2013, 2015, 2018, 2019) track with the same physics assumptions as in Jin et al. (2025), except for the wind \dot{M} rates (see Jin et al. (2024) for details). In test hydrodynamic simulations the RLOF material was found to disperse after $\lesssim 50$ kyr, setting an upper limit for the timescale of depletion of surface H after a RLOF event. O stars are expected to retain some surface H after rapid RLOF in an intermediate slow RLOF phase for $\gtrsim 100$ kyr (Clark et al. 2014), which would appear as e.g. a WN9h spectral type, so this favours an evolutionary path with multiple RLOF episodes. One model with two RLOF events was identified in the grid of Jin et al. (2025) which was close to the known age, luminosity (L_{bol}) and P of Wd1-72, but was H free after ~ 70 kyr. This model is at Solar metallicity, has an initial P of 3.98 d, primary (initially more massive) $M_{\text{init}} = 28.18 M_{\odot}$ and secondary $M_{\text{init}} = 19.73 M_{\odot}$. We reran this evolutionary track with a factor 4.7 increase in the \dot{M} of the primary star starting immediately after the second RLOF event, to approximately match the rate of $9 \times 10^{-5} M_{\odot} \text{ yr}^{-1}$ measured from spectra of Wd1-72 by Rosslowe (2015). This model reaches a surface H abundance of $\sim 1\%$ only ~ 20 kyr post-RLOF (see left panel of Fig. 1) and was used in our hydrodynamic simulation. We compare this MESA track with Wd1-72 in App. A.

2.2. Hydrodynamic model

We performed our simulations using the (magneto)hydrodynamic code PION (Mackey et al. 2021). Unless otherwise noted, the simulation setup and parameters used are as for the simulation presented in Larkin et al. (2025b). In particular, we assume full photoionization due to the intense extreme-ultraviolet (EUV) radiation field ionising cool circumstellar material near the cluster core (Andrews et al. 2018), include radiative heating and cooling with model 8 of PION as described in Green et al. (2019), and do not include a magnetic field. We use six levels of static mesh refinement for the simulation, using a 2D rectangular domain $D(r, z)$ of $r \in [0, 10.0 \times 10^{18}] \text{ cm}$, $z \in [-10.0 \times 10^{18}, 10.0 \times 10^{18}] \text{ cm}$. D is fully covered at level $n = 0$ and each subsequent level of refinement covers a sub-domain of diameter $D/2^n$. We use 512×256 grid cells per level of refinement, such that the finest grid resolution is $\Delta x = 2.44 \times 10^{15} \text{ cm}$.

We assume a constant cluster wind of $v_z = -1500 \text{ km s}^{-1}$, density $1 \times 10^{-24} \text{ g cm}^{-3}$ and pressure $5 \times 10^{-9} \text{ dyn cm}^{-2}$ (Larkin et al. 2025a,b). We use the MESA evolutionary track described above as input for the source term in our hydrodynamic model, with a wind injection radius of $5 \times 10^{16} \text{ cm}$ (~ 20 cells). We begin the simulation at 6.779 Myr to establish a pre-RLOF stellar bubble, and run it until 6.82 Myr, by which time the RLOF

material has left the domain. We use the \dot{M} value of the primary star throughout the simulation, assuming fully non-conservative mass transfer. We calculate the stellar wind velocity (v_{∞}) from the MESA track by scaling the primary star's escape velocity by the T_{eff} -dependent prescription of Eldridge et al. (2006) except for during RLOF where we use a fixed value of 20 km s^{-1} (Scherbak et al. 2025). We show the evolution of these values along with P in the left panel of Fig. 1.

3. Results

We show four key stages in the simulation evolution in the right panel of Fig. 1. The first panel shows RLOF material filling the pre-RLOF stellar bubble. The second panel shows the WR wind expanding into the RLOF material, with Rayleigh-Taylor (RT) fingers developing. The RLOF material asymmetry arises from the cluster wind. The third panel shows the now fragmented RLOF material as small, quasi-spheroidal droplets in the $+z$ direction in the wake of the ejecta standoff bow shock (see App. B). In the $-z$ direction, the structure is more filamentary. At the end of the simulation, in the final panel, these filaments have separated into cometary-like droplets with tails. The spheroidal droplets disperse radially from the star on ballistic trajectories, whereas the cometary droplets are starting to be carried away in the cluster wind. This fragmentation is dependent on the simulation spatial resolution, with higher resolution leading to more efficient and rapid fragmentation. For the $+z$ half of the domain we find a total mass in clumps $M_{\text{cl}} = 7.3 \times 10^{-3} M_{\odot}$ and average clump density $\rho_{\text{cl}} = 8.8 \times 10^{-22} \text{ g cm}^{-3}$. For the $-z$ half we obtain $M_{\text{cl}} = 3.8 \times 10^{-2} M_{\odot}$ and $\rho_{\text{cl}} = 2.9 \times 10^{-22} \text{ g cm}^{-3}$.

In Fig. 2 we compare the density field of our simulation with the JWST F1130W data towards Wd1-72. In the direction towards the cluster core we observe quasi-spheroidal droplets in the data, which we also find in our simulation. In the opposite direction, the material around Wd1-72 is structured in droplets with cometary-like tails. These tails point away from the star as opposed to the cluster core (as seen elsewhere in Wd 1), which is also reproduced by our simulation. The main difference is the non-uniformity of the cometary tail distribution in the data, with the upper part of the figure being more sparsely populated than the lower part. We do not observe this kind of spatial variability in our simulation. The material appears to be more filamentary towards the bottom, whereas more distinct droplets with tails are seen towards the top. We observe both of these morphologies in our simulation, but not at the same time. Finally, the material in the observations appears to be a factor ~ 2 closer to Wd1-72 than in our simulations. This can be at least partially accounted for by the resolution dependence of the fragmentation, and the 2D nature of our simulation, as fragmentation would be more efficient in 3D. These results also depend on our assumptions of the density and velocity of both the stellar and cluster wind.

4. Discussion & Conclusions

In this letter we demonstrate that the complex nebulosity surrounding Wd1-72 can be explained via intense \dot{M} characteristic of non-conservative RLOF being fragmented by a WR wind and carried away in a cluster wind. This scenario should not strongly depend on the specific stellar evolution track, and we stress that the MESA track used here is only one possibility. The WN7 subtype favours this putative RLOF event being a second or subsequent one, as complete H removal in a single RLOF event is unlikely to occur before the droplets are dispersed.

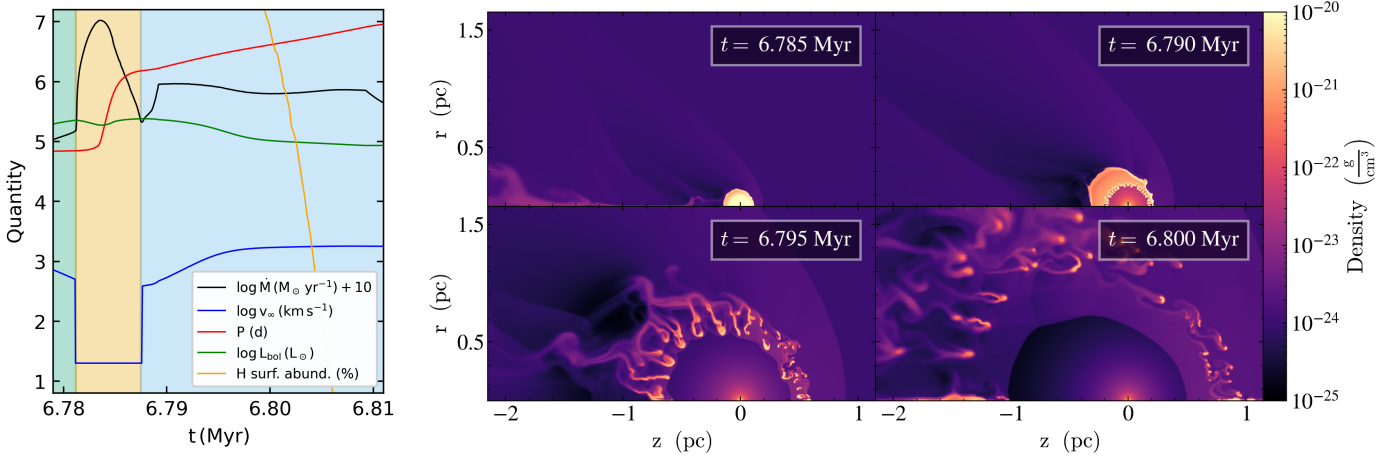


Fig. 1: Left: Evolution of \dot{M} , v_{∞} , P , L_{bol} and surface H abundance in our MESA track. The green, yellow and blue panels correspond to pre-RLOF, RLOF and WR wind phases. Right: Density slices for four key stages in the evolution of our simulation, with the cluster wind moving in the $-z$ direction.

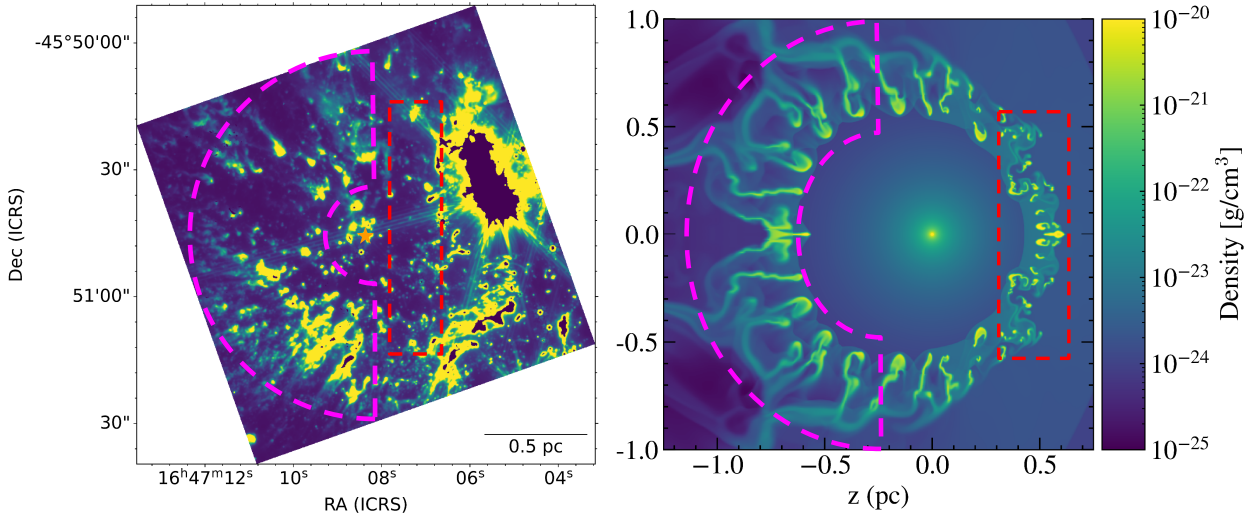


Fig. 2: Left: JWST/MIRI F1130W observations towards Wd1-72, which is marked with an orange star. Right: Density slice from our simulation mirrored around the z -axis at $t = 6.795 \text{ Myr}$. We highlight the regions of spheroidal droplets in red, and comet-like droplets pointing towards Wd1-72 in pink, demonstrating the qualitative correspondence between the data and simulation.

The most significant simplifying assumption we have made is a spherically symmetric outflow from Wd1-72. While an equatorial outflow would arguably be more realistic (e.g. Scherbak et al. 2025), our results would then be sensitive to the (presently unknown) system orientation with respect to the cluster wind. This difference in geometry could account for the non-uniform distribution of material around Wd1-72. We further assumed a fixed RLOF outflow velocity of 20 km s^{-1} , consistent with values of a few tens of km s^{-1} expected for close massive binary systems (Scherbak et al. 2025). Given the high L/M and extended radii for the new WR immediately post-mass transfer, which both exceed values predicted for He main sequence stars, we expect an enhanced wind mass-loss rate (e.g., Sander et al. 2020, 2023), in line with our adjusted MESA model. Finally, we did not consider radiation pressure accelerating the dusty RLOF material, which is expected to be negligible at scales $\gtrsim 0.1 \text{ pc}$.

It has been suggested that rapidly rotating WR stars can be produced by LBV eruptions (Vink et al. 2011). However, ejecta nebulae around WR stars are rarely associated with bi-

nary central stars (Stock & Barlow 2010) and we demonstrate in App. B that a typical giant eruption mass-loss rate of order $0.1 M_{\odot} \text{ yr}^{-1}$ is incompatible with the ejecta morphology, which requires eruptive \dot{M} to be a few $10^{-4} M_{\odot} \text{ yr}^{-1}$ at most. Given the WN7 subtype, this degree of H stripping from a minor eruption ($\lesssim 0.5 M_{\odot}$) is disfavoured.

Additional observations will greatly aid efforts to understand the outflows in Wd 1, especially around Wd1-72 as existing NIRCam JWST data here are badly saturated and affected by diffraction spikes. Integral field spectroscopy would probe the physical conditions, line-of-sight velocities, compositions and inclination angle of the droplets around Wd1-72, testing our proposed evolutionary scenario. An additional epoch of imaging with e.g. JWST/MIRI would provide proper motion measurements of the droplets constraining both the currently unknown transition timescale from sgB[e] to newly-emerged WR binary and Wd 1's collective wind velocity. Finally, multi-epoch medium resolution optical/NIR spectra would probe which of the two X-ray periodicities is that of the binary system. This

could also provide the rotational velocity of the secondary, which should have been significantly spun up if mass-transfer happened recently.

If Wd1-72 is exiting a phase of recent mass-transfer, it suggests that unstable mass-transfer occurs in short period WN binaries. Considering that >90% of Wd 1's WR stars are in binaries, it would also add to the growing body of evidence that binary interactions are important for WR evolution at all metallicities. We conclude that:

- The complex morphology of nebulosity in the vicinity of Wd1-72 can be reproduced by non-conservative RLOF mass-loss followed by a Wolf-Rayet stellar wind expanding into a cluster wind.
- Follow-up observations of Wd1-72 and the nearby material are needed to test whether this material is from RLOF mass-loss, if the system is a short-period binary, and if the companion has been spun up.
- If Wd1-72 and Wd1-9 represent different evolutionary stages of recent post-interaction WN binaries, then this could resolve the question of how such systems form, improving our understanding of gravitational wave binary progenitor systems.

Acknowledgements. The authors thank P.A. Crowther, A. Gilkis, M. Gronke, M. Mapelli, F.R.N. Schneider and J.S. Vink for discussions. CJKL gratefully acknowledges support from the International Max Planck Research School for Astronomy and Cosmic Physics at the University of Heidelberg in the form of an IMPRS PhD fellowship. AACCS, RRL and CJKL are supported by the Deutsche Forschungsgemeinschaft (DFG, German Research Foundation) in the form of an Emmy Noether Research Group – Project-ID 445674056 (SA4064/1-1, PI Sander). This project was co-funded by the European Union (Project 101183150 - OCEANS). TJH acknowledges a Dorothy Hodgkin Fellowship, UKRI guaranteed funding for a Horizon Europe ERC consolidator grant (EP/Y024710/1) and UKRI/STFC grant ST/X000931/1. A.B acknowledges support from the Deutsche Forschungsgemeinschaft (DFG, German Research Foundation) under Germany's Excellence Strategy – EXC 2094 – 390783311. FN gratefully acknowledges support by grant PID2022-137779OB-C41 funded by the Spanish Ministry of Science, Innovation and Universities/State Agency of Research MICIU/AEI/10.13039/501100011033 and by "ERDF A way of making Europe". E.S. is supported by the international Gemini Observatory, a program of NSF NOIRLab, which is managed by the Association of Universities for Research in Astronomy (AURA) under a cooperative agreement with the U.S. National Science Foundation, on behalf of the Gemini partnership of Argentina, Brazil, Canada, Chile, the Republic of Korea, and the United States of America. The simulations presented here were performed on the HPC system Raven at the Max Planck Computing and Data Facility. This research has made use of the Astrophysics Data System, funded by NASA under Cooperative Agreement 80NSSC21M00561. This study used these software packages: PION (Mackey et al. 2021), pypion (Green & Mackey 2021), Numpy (Harris et al. 2020), matplotlib (Hunter 2007), yt (Turk et al. 2011), TORUS (Harries et al. 2019).

References

Anastasopoulou, K., Guarcello, M. G., Drake, J. J., et al. 2025, A&A, 701, A138

Anastasopoulou, K., Guarcello, M. G., Flaccomio, E., et al. 2024, A&A, 690, A25

Andrews, H., Fenech, D., Prinja, R. K., Clark, J. S., & Hindson, L. 2018, MNRAS, 477, L55

Beasor, E. R., Davies, B., Smith, N., Gehrz, R. D., & Figer, D. F. 2021, ApJ, 912, 16

Boffin, H. M. J., Rivinius, T., Mérard, A., et al. 2016, A&A, 593, A90

Bonanos, A. Z. 2007, AJ, 133, 2696

Castellanos, R. et al. in prep.

Clark, J. S., Munoz, M. P., Negueruela, I., et al. 2008, A&A, 477, 147

Clark, J. S., Ritchie, B. W., Najarro, F., Langer, N., & Negueruela, I. 2014, A&A, 565, A90

Clark, J. S., Ritchie, B. W., & Negueruela, I. 2020, A&A, 635, A187

Conti, P. S. 1975, Memoires of the Societe Royale des Sciences de Liege, 9, 193

Conti, P. S. & Massey, P. 1989, ApJ, 337, 251

Crowther, P. A., Hadfield, L. J., Clark, J. S., Negueruela, I., & Vacca, W. D. 2006, MNRAS, 372, 1407

de Mink, S. E., Sana, H., Langer, N., Izzard, R. G., & Schneider, F. R. N. 2014, ApJ, 782, 7

Draine, B. T. 2003, ARA&A, 41, 241

Dsilva, K., Shenar, T., Sana, H., & Marchant, P. 2023, A&A, 674, A88

Ekström, S., Georgy, C., Eggenberger, P., et al. 2012, A&A, 537, A146

Eldridge, J. J., Genet, F., Daigne, F., & Mochkovitch, R. 2006, MNRAS, 367, 186

Green, S. & Mackey, J. 2021, PyPion: Post-processing code for PION simulation data, Astrophysics Source Code Library, record ascl:2103.026

Green, S., Mackey, J., Haworth, T. J., Gvaramadze, V. V., & Duffy, P. 2019, A&A, 625, A4

Groh, J. H., Meynet, G., Ekström, S., & Georgy, C. 2014, A&A, 564, A30

Guarcello, M. G., Almendros-Abad, V., Lovell, J. B., et al. 2025, A&A, 693, A120

Harries, T. J., Haworth, T. J., Acreman, D., Ali, A., & Douglas, T. 2019, Astronomy and Computing, 27, 63

Harris, C. R., Millman, K. J., van der Walt, S. J., et al. 2020, Nature, 585, 357

Higgins, E. R., Sander, A. A. C., Vink, J. S., & Hirschi, R. 2021, MNRAS, 505, 4874

Hirai, R., Podsiadlowski, P., Owocki, S. P., Schneider, F. R. N., & Smith, N. 2021, MNRAS, 503, 4276

Hunter, J. D. 2007, Computing in Science & Engineering, 9, 90

Jin, H., Langer, N., Ercolino, A., & de Mink, S. E. 2025, arXiv e-prints, arXiv:2510.19965

Jin, H., Langer, N., Lennon, D. J., & Proffitt, C. R. 2024, A&A, 690, A135

Langer, N., Hamann, W. R., Lennon, M., et al. 1994, A&A, 290, 819

Larkin, C. J. K., Hawcroft, C., Mackey, J., et al. 2025a, A&A, 703, L14

Larkin, C. J. K., Mackey, J., Haworth, T. J., & Sander, A. A. C. 2025b, A&A, 700, A60

Mackey, J., Green, S., Moutzouri, M., et al. 2021, MNRAS, 504, 983

Marchant, P. & Bodensteiner, J. 2024, ARA&A, 62, 21

Paczyński, B. 1967, Acta Astron., 17, 355

Paxton, B., Bildsten, L., Dotter, A., et al. 2011, ApJS, 192, 3

Paxton, B., Cantiello, M., Arras, P., et al. 2013, ApJS, 208, 4

Paxton, B., Marchant, P., Schwab, J., et al. 2015, ApJS, 220, 15

Paxton, B., Schwab, J., Bauer, E. B., et al. 2018, ApJS, 234, 34

Paxton, B., Smolec, R., Schwab, J., et al. 2019, ApJS, 243, 10

Portegies Zwart, S. F., McMillan, S. L. W., & Gieles, M. 2010, ARA&A, 48, 431

Rosslowe, C. 2015, PhD thesis, University of Sheffield, UK

Sabbahit, G. N., Vink, J. S., Higgins, E. R., & Sander, A. A. C. 2022, MNRAS, 514, 3736

Sana, H., de Mink, S. E., de Koter, A., et al. 2012, Science, 337, 444

Sander, A. A. C., Lefever, R. R., Josiek, J., et al. 2025, Nature Astronomy [arXiv: 2508.18410]

Sander, A. A. C., Lefever, R. R., Poniatowski, L. G., et al. 2023, A&A, 670, A83

Sander, A. A. C., Vink, J. S., & Hamann, W. R. 2020, MNRAS, 491, 4406

Scherbak, P., Lu, W., & Fuller, J. 2025, ApJ, 990, 172

Stock, D. J. & Barlow, M. J. 2010, MNRAS, 409, 1429

Turk, M. J., Smith, B. D., Oishi, J. S., et al. 2011, The Astrophysical Journal Supplement Series, 192, 9

Vink, J. S., Gräfener, G., & Harries, T. J. 2011, A&A, 536, L10

¹ Max-Planck-Institut für Kernphysik, Saupfercheckweg 1, D-69117 Heidelberg, Germany
e-mail: cormac.larkin@mpi-hd.mpg.de

² Zentrum für Astronomie der Universität Heidelberg, Astronomisches Rechen-Institut, Mönchhofstr. 12-14, 69120 Heidelberg, Germany

³ Max-Planck-Institut für Astronomie, Königstuhl 17, D-69117 Heidelberg, Germany

⁴ Astronomy & Astrophysics Section, School of Cosmic Physics, Dublin Institute for Advanced Studies, DIAS Dunsink Observatory, Dublin D15 XR2R, Ireland

⁵ Max Planck Institute for Astrophysics, Karl-Schwarzschild-Str. 1, 85748 Garching, Germany

⁶ Universität Heidelberg, Interdisziplinäres Zentrum für Wissenschaftliches Rechnen, 69120 Heidelberg, Germany

⁷ Istituto Nazionale di Astrofisica (INAF) – Osservatorio Astronomico di Palermo, Piazza del Parlamento 1, 90134 Palermo, Italy

⁸ European Southern Observatory, Karl-Schwarzschild-Strasse 2, 85748 Garching bei München, Germany

⁹ Lockheed Martin Solar and Astrophysics Laboratory, 3251 Hanover Street, Palo Alto, CA 94304, USA

¹⁰ School of Physical and Chemical Sciences, Queen Mary University of London, Mile End, London E1 4NS, UK

¹¹ Gemini Observatory/NSFs NOIRLab, 950 N. Cherry Ave., Tucson, AZ 85719, USA

¹² Departamento de Astrofísica, Centro de Astrobiología, CSIC-INTA, Ctra. Torrejón a Ajalvir km 4, E-28850 Torrejón de Ardoz, Spain

¹³ Department of Physics and Astronomy, The Open University, Walton Hall, Milton Keynes MK7 6AA, UK

Appendix A: MESA track

Here we address the compatibility of our assumed MESA track with the known age, luminosity, period and surface H abundance of Wd1-72. Our track is 6.8 Myr post-ZAMS which is comparable to the cluster age of ~ 6 Myr found by [Castellanos et al. \(in prep.\)](#). [Rosslowe \(2015\)](#) derive a luminosity of $\log L = 5.45$ for the WR star. Our MESA track has a value of $\log L = 5.0$ for $t = 6.80$ Myr, but this difference can be accounted for by the choice of extinction law in [Rosslowe \(2015\)](#) and the poorly constrained contribution of the secondary star. Our MESA track has $P = 6.6$ d at $t = 6.80$ Myr, and reaches 6.9 d at $t = 6.81$ Myr. At $t = 6.80$ Myr in the MESA track, surface H abundance is less than 10%, with depletion to 1% being reached at $t \sim 6.805$ Myr.

There is a mild discrepancy between the time when the droplet morphology corresponds well with the observations ($t \sim 6.80$ Myr) and when the MESA track orbital period and surface H abundance best match the measured properties of Wd1-72 ($t \sim 6.81$ Myr). At this later time we observe the droplets are blown out of the simulation domain by the cluster wind.

Appendix B: Physical constraints on the eruption

Here we demonstrate analytically that a giant LBV eruption cannot account for the observations around Wd1-72. Assuming an eruption instead of RLOF \dot{M} , the fragmentation can only occur when the ram-pressures of the eruption and cluster wind are approximately balanced, creating a standoff bow shock. RT fingers would then develop in the wake of this bow shock. From the data we see the standoff distance would be at $d \sim 0.5$ pc from the star. We can balance the ram-pressures to obtain the ejection wind density ρ_E at d :

$$\rho_E = 2.5 \times 10^{-23} \cdot \left(\frac{\rho_{CW}}{10^{-24} \text{ g cm}^{-3}} \right) \left(\frac{v_{CW}}{10^3 \text{ km s}^{-1}} \right)^2 \left(\frac{v_E}{200 \text{ km s}^{-1}} \right)^{-2} \text{ g cm}^{-3}$$

Where ρ_{CW} , v_{CW} and v_E are the cluster wind density, cluster wind velocity and eruption velocity respectively. Applying the continuity equation, the equivalent eruption \dot{M} for this density can be expressed as:

$$\dot{M}_E = 4\pi d \rho_E v_E = 2.37 \times 10^{-4} \left(\frac{\rho_{CW}}{10^{-24} \text{ g cm}^{-3}} \right) \left(\frac{v_{CW}}{10^3 \text{ km s}^{-1}} \right)^2 \left(\frac{v_E}{200 \text{ km s}^{-1}} \right)^{-1} \left(\frac{d}{0.5 \text{ pc}} \right) M_\odot \text{ yr}^{-1}$$

For reasonable choices of these parameters, it is clear \dot{M} must be of order a few $10^{-4} M_\odot \text{ yr}^{-1}$ at most for the ejecta to fragment in the cluster wind at this distance, assuming $v_E \sim 200 \text{ km s}^{-1}$. Higher \dot{M} is only possible if v_E is around an order of magnitude less, such as for RLOF. In this case, a dense shell of CSM develops during the RLOF phase, which is then fragmented from within via RT instabilities driven by the WR wind. We see this mechanism operating in Fig. B.1, where we show a slice of z -axis velocity (v_z) from our simulation.

The droplets towards the cluster wind have expansion velocities $v_{\text{exp}} = \sqrt{v_z^2 + v_r^2}$ of order $\lesssim 50 \text{ km s}^{-1}$ as they are at the

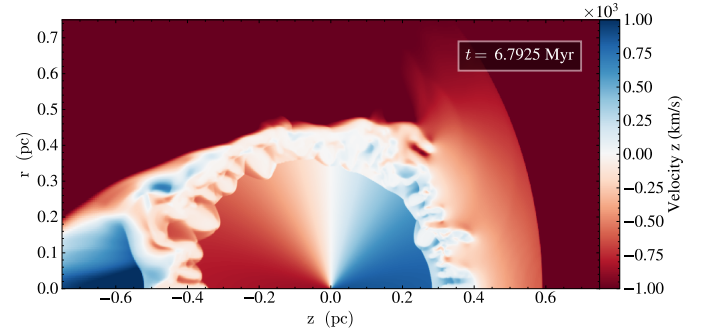


Fig. B.1: Simulation slice of z -axis velocity at 6.7925 Myr.

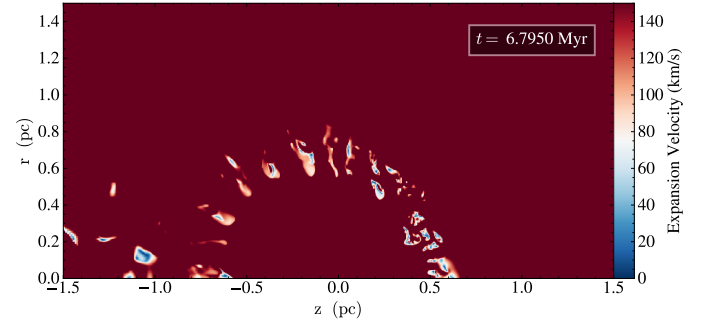


Fig. B.2: Simulation slice of expansion velocity at 6.795 Myr.

stagnation point of the flow and so are decelerated. The downstream droplets are accelerated by the WR wind and/or cluster wind, whichever impacts them. We show a slice of v_{exp} in Fig. B.2.

Appendix C: Dust emission from dense clumps

We used the TORUS Monte Carlo radiative transfer code ([Harries et al. 2019](#)) to calculate thermal dust emissivity and dust temperature in the droplets produced by our simulation. We assume a constant 1% dust mass-fraction for the RLOF material, and that the fast stellar winds and the cluster wind are dust free. We use the same TORUS settings as [Larkin et al. \(2025b\)](#), specifically assuming silicate grains ([Draine 2003](#)) and a grain-size distribution with power-law index of -3.3 from 0.005 to $0.2 \mu\text{m}$.

We added six radiation sources, all of which are at $R = 0$ along the z -axis, imposed because of symmetry constraints of the 2D simulations. Wd1-72 is treated as a source with $\log_{10} L/L_\odot = 5.45$ and 65 kK at $z = 0$ pc, the core of Wd 1 with $\log_{10} L/L_\odot = 5.9$, $T = 40$ kK at $z = 1$ pc, WR U with $\log_{10} L/L_\odot = 5.5$, $T = 38$ kK at $z = 0.5$ pc, two sources representing nearby (in projection) WR stars with $\log_{10} L/L_\odot = 5.2$, $T = 50$ kK at $z = 0.48$ and 0.52 pc, and a source in the downstream region with $\log_{10} L/L_\odot = 5.5$, $T = 7.5$ kK at $z = -0.25$ pc.

Results of the TORUS modelling are shown in Fig. C.1, where we plot dust emissivity ϵ (the TORUS variable `etacont`, already multiplied by wavelength and so with units $\text{erg cm}^{-3} \text{ s}^{-1}$) in the upper half-plane and dust temperature in the lower half-plane. We did not calculate emission maps because the rotational symmetry imposed by the 2D simulation converts all features into rings.

Looking at T_{dust} , the droplets towards the core of Wd 1 are warmer than those in the downstream direction, as expected due

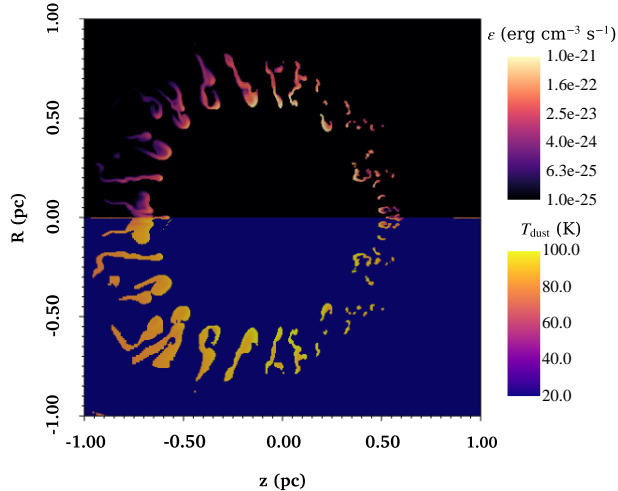


Fig. C.1: Upper half plane: thermal dust emissivity (ϵ) at $t = 6.795$ Myr calculated with the TORUS radiative transfer code, calculated at $\lambda = 11\mu\text{m}$ in units of $\text{erg cm}^{-3} \text{s}^{-1}$. Lower half-plane: dust temperature (T_{dust}) assuming radiative equilibrium, where blue regions are dust-free and so the temperature is not defined.

to the intense cluster radiation field. The tails of the globules (at $z < -0.5\text{ pc}$) are even cooler and their emission at $11\mu\text{m}$ is faint in comparison to the rest of the dusty material. Comparing with Fig. 2 the same morphology is seen in the *JWST* image. We cannot quantitatively compare the brightness of simulated dust emission with observations without a 3D simulation, which is currently too computationally expensive to justify given the large uncertainties in the mass and expansion velocity of the droplets and globules.